Fully Optical Modulation of the Two-Dimensional Electron Gas at the γ-Al$_2$O$_3$/SrTiO$_3$ Interface

Wei Niu,[○] Yue-Wen Fang,[○] Ruxin Liu,[○] Zhenqi Wu, Yongda Chen, Yulin Gan, Xiaoqian Zhang, Chunhui Zhu, Lixia Wang, Yongbing Xu, Yong Pu,* Yunzhong Chen,* and Xuefeng Wang*

ACCESS | 📊 Metrics & More | 📖 Article Recommendations | 🆂🅸 Supporting Information

ABSTRACT: Two-dimensional electron gas (2DEG) formed at the heterointerface between two oxide insulators hosts plenty of emergent phenomena and provides new opportunities for electronics and photoelectronics. However, despite being long sought after, on-demand properties controlled through a fully optical illumination remain far from being explored. Herein, a giant tunability of the 2DEG at the interface of γ-Al$_2$O$_3$/SrTiO$_3$ through a fully optical gating is discovered. Specifically, photon-generated carriers lead to a delicate tunability of the carrier density and the underlying electronic structure, which is accompanied by the remarkable Lifshitz transition. Moreover, the 2DEG can be optically tuned to possess a maximum Rashba spin−orbit coupling, particularly at the crossing region of the sub-bands with different symmetries. First-principles calculations essentially well explain the optical modulation of γ-Al$_2$O$_3$/SrTiO$_3$. Our fully optical gating opens a new pathway for manipulating emergent properties of the 2DEGs and is promising for on-demand photoelectric devices.
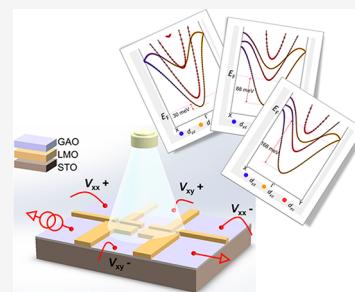
Two-dimensional electron gas (2DEG) formed at the heterointerface, particularly LaAlO$_3$/SrTiO$_3$ (LAO/STO), exhibits a variety of extraordinary properties and functionalities, such as high carrier mobility,[1,2] Rashba spin−orbit coupling (SOC),[3,4] spin polarization,[5] superconductivity,[6] quantum transport,[7−9] and high-efficiency spin-charge interconversion.[10−12] A further intriguing feature is that these emergent states can be significantly tuned via multistimuli,[13] including strain,[14] electrostatic gating,[15] light irradiation,[16,17] and chemical doping.[18,19] In particular, extensive attempts have been devoted to tailor transport properties via the electrostatic gating. For instance, due to the large permittivity of STO and KTaO$_3$ substrates, back-gate configurations are generally applied to investigate the electrostatic field effect on the sheet resistance,[20] carrier mobility,[21] metal−insulator transition,[22] electronic structure,[15,23] Rashba SOC,[3,24] and superconductivity.[25] However, for conventional electrostatic gating, high voltages of tens to hundreds of volts are required to gain a sizable field effect.[22,26] Under such high voltages and sufficiently long time, it is very likely to induce defects such as oxygen vacancies,[20] which may destroy the expected emergent states.

Optical gating (i.e., light illumination) is an alternative way to tune the emergent properties in oxides. It has been demonstrated to be a powerful means of inducing or enhancing superconductivity,[27] metal−insulator transition,[28] ferromagnetism,[29] quantum oscillation,[30] and spin manipulation.[31] Moreover, oxide 2DEGs have been found to be strongly coupled and sensitive to light illumination,[13] which develops a giant photoinduced-persistent photoconductivity (PPC) at the STO-based interfaces.[32,33] This inspires us to design photo-electronic devices on the basis of oxide 2DEGs. However, most of the previous studies focused on the photoinduced change in resistance,[34,35] rather than the fundamentally intrinsic properties, such as carrier density, electronic structure, mobility, and the corresponding effects. To reveal the underlying mechanism of the sensitivity to light exposure, it is necessary to investigate the optical gating on the carrier density and electronic structures, but such research remains scarce. Recently, when electrostatic gating is combined with an optical gating of some specific wavelengths, it is found that 2DEGs undergo some changes, for instance, light-enhanced lattice polarizations[16] and tunable Rashba SOC.[36,37] Notably, all-optical tunability of the ground states of 2DEGs without the assistance of the electrostatic gating remains under-investigated, which could be promising for on-demand photoelectric devices.

For the STO-based 2DEGs, conduction bands of STO contribute to the interfacial electronic structures, which are bent toward the interface and cross the Fermi level.[38] Therefore, the modulation of the Fermi level and electronic structure can be expected to induce a series of novel properties. The electronic structure of the LAO/STO systems has been intensively investigated via electrostatic gating.[15,38] In addition, beyond the LAO/STO heterointerface, 2DEG formed at the
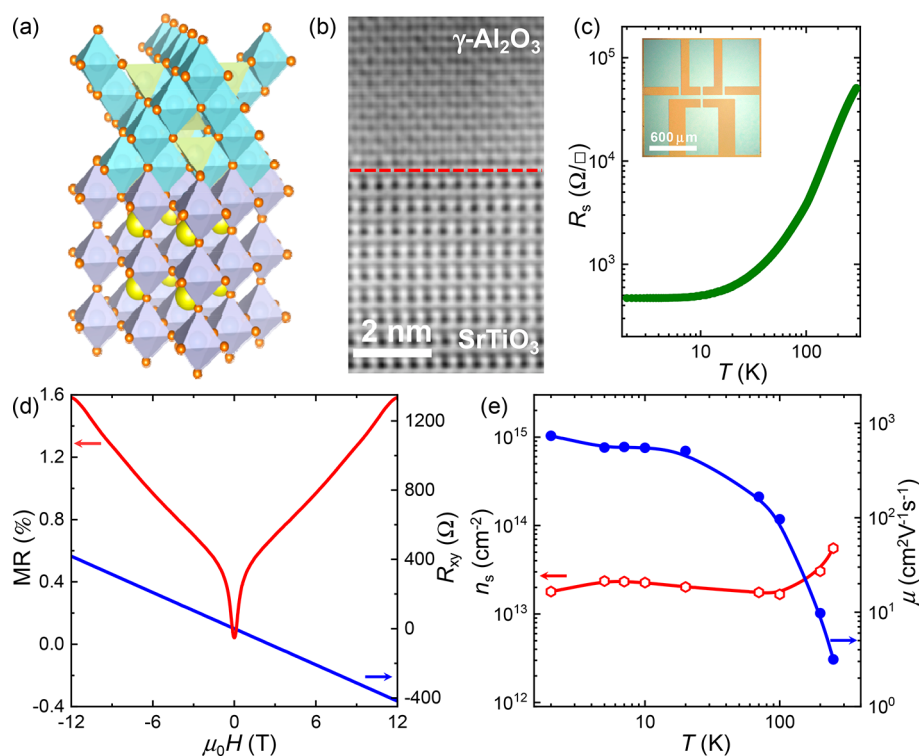
Figure 1. (a) Schematic illustration of the non-isostructural heterointerface of GAO/STO. (b) ABF-STEM image of the GAO/STO heterointerface. (c) Temperature-dependent sheet resistance of the GAO/STO device before optical gating. The inset shows the optical image of the Hall-bar device. (d) Magnetoresistance (MR) and Hall resistance (R_{xy}) with respect to the applied magnetic field at 2 K. (e) Temperature dependence of the carrier density and mobility of the pristine sample without illumination.

non-isostructural interface of spinel/perovskite γ-Al$_2$O$_3$/STO (GAO/STO) has received extensive interest due to its more extraordinary properties. For instance, the mobility of GAO/STO has been promoted over 2 orders of magnitude compared with that of the LAO/STO paradigm.[39] Regarding this extremely high mobility, GAO/STO is expected to achieve the highest efficiency for the spin-to-charge conversion.[40] Moreover, a long-range magnetic order evidenced as magnetic stripes rather than magnetic patches observed in LAO/STO has been demonstrated in the GAO/STO heterointerface. More remarkably, this long-range magnetic order shows an effective modulation when applying stress.[41] Ground states of the GAO/STO heterointerface can be effectively tuned, albeit via ionic-liquid electrostatic gating.[26] Nevertheless, optical gating on the underlying electronic structures of 2DEGs remains at an early stage of investigation, especially for fully optical gating (without the assistance of electrostatic gating). Whether the optical gating could achieve the comparatively giant tunability in 2DEGs as that by electrostatic gating remains an open question. Therefore, it is interesting and promising to manipulate 2DEG at the spinel/perovskite interface of GAO/STO via fully optical gating. Furthermore, an unusual energy ordering of orbitals, i.e., the anomalous upward shift of the d$_{xy}$ states over the d$_{xz}$/d$_{yz}$ ones, was proposed recently in GAO/STO,[42−44] presenting a strikingly different electronic structure from the one of LAO/STO. This has not yet been well understood because of the complexity of the GAO/STO interface. Moreover, one doubts whether the great tunability of oxide interfaces could reproduce in GAO/STO with this anomalous band structure. In this work, we investigate fully optical gating on transport properties of 2DEG at the GAO/STO interface and deepen the understanding of

its band structure and the resultant experimental phenomena supported by the first-principles theory. Tuning the carrier density continuously by changing the wavelength of the applied light alone, we observe the light-tailored intrinsic band structure of GAO/STO. Consequently, 2DEG undergoes the remarkable Lifshitz transition and experiences the maximum Rashba SOC, accompanied with an enhanced conducting state. Our fully optical gating opens a new pathway for manipulating the emergent properties of the 2DEGs and is promising for all-oxide photoelectric device applications.

Despite the distinct lattice structures between GAO and STO, epitaxial growth can be achieved for the spinel/perovskite heterostructure, as schematically depicted in Figure 1a. The high quality of the interface is verified by the high-resolution transmission electron microscopy (TEM). Figure 1b shows the annular bright-field (ABF) scanning transmission electron microscopy (STEM) image of the corresponding GAO/STO interface. It is obvious that the interface is atomically sharp without any dislocations. To conduct accurate transport measurements, the GAO/STO interface was patterned into Hall-bar devices using LaMnO$_3$ (LMO) as the hard mask as previously reported,[26] and more details can refer to Figure S1. The inset of Figure 1c shows the optical image of a Hall-bar device. Before applying the optical gating, the prime transport properties of the 2DEG were measured initially. It should be noted that, to get access to the intrinsic properties and to eliminate the perturbation from the photocarrier, GAO/STO devices were shielded from any light over 24 h before the measurements.[13,45] As shown in Figure 1c, the pristine GAO/STO interface shows a typical metallic behavior, i.e., the sheet resistance (R_s) decreases from ∼51 000 to ∼470 Ω/□ upon cooling from 300 to 2 K.
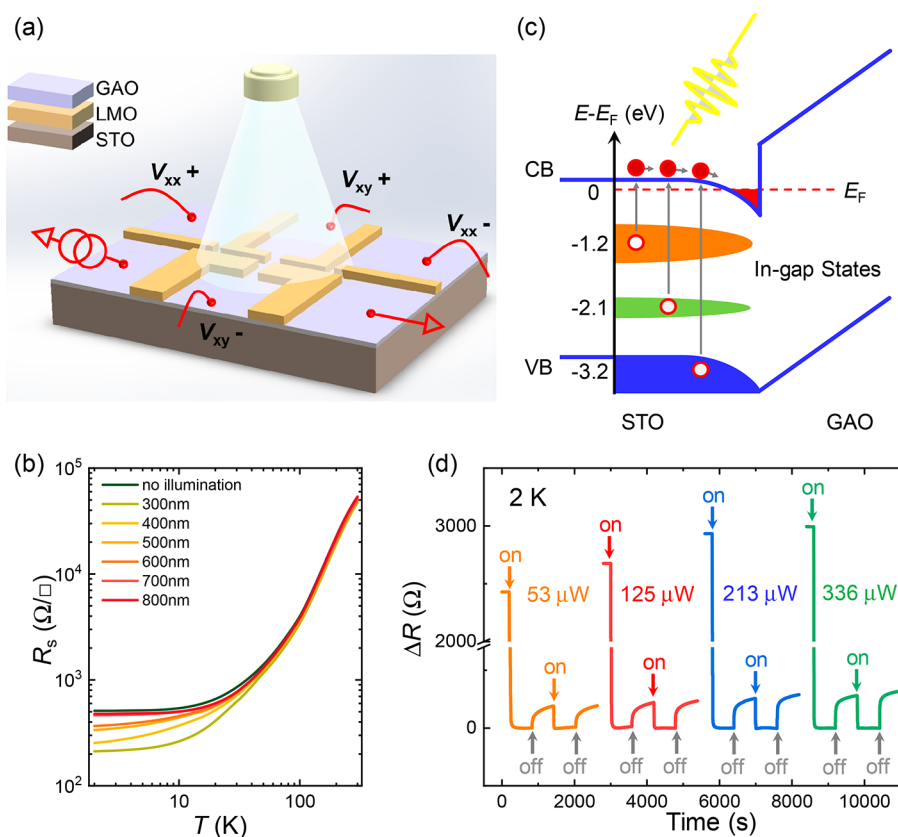
Figure 2. (a) Measurement configuration for the optical modulation of the 2DEG at the GAO/STO interface. (b) Optical modulation of the sheet resistance, R_s, of the GAO/STO heterointerface. (c) The underlying mechanism of the optical gating. When the optical gating is adopted, the photogenerated electrons are excited from in-gap states or the valence band to the conductance band of STO and then accumulated in the potential well of the 2DEG. (d) Photoinduced relative change in resistance (ΔR) as a function of time under various light powers at 2 K (λ= 300 nm).

Figure 1d depicts the typical magnetoresistance (MR) and Hall resistance (R_{xy}) at 2 K. Remarkably, a prominent observation is the sharp cusps at low magnetic field, which is the most salient characteristic of the weak antilocalization (WAL) effect.[26] The WAL effect stems from the destructive interference of electron waves propagating in time-reversal closed trajectories induced by the Rashba SOC.[3,37] Besides the WAL effect around the zero magnetic field, a positive parabolic MR curve is observed in the whole magnetic field range. The MR ratio, defined as MR = $(R_{xx}(\mu_0 H) - R_{xx}(0))/R_{xx}(0) \times$ 100%, is 1.6% when T = 2 K, which is comparable to the ones in previous 2DEG systems.[46,47] Furthermore, the magnetic field-dependent R_{xy} is linear, implying only one type of carrier dominates the transport. Under this circumstance, carrier density, n_s, can be deduced easily using the formula: $n_s = -1/R_H \cdot e$, where R_H is the Hall coefficient. Subsequently, n_s and mobility (μ) as a function of the temperature are summarized in Figure 1e. The n_s at 250 K is 5.6×10^{13} cm^{-2}. It decreases with the decline of temperature and keeps a constant around 2×10^{13} cm^{-2} at low temperatures. This temperature-dependent n_s behavior indicates a carrier freezing-out effect, which is ascribed to the in-gap states from the oxygen vacancies and frequently observed in the oxygen-deficient 2DEG systems.[48,49] On the other hand, the carrier mobility decreases from ~736 cm^{2}V^{-1}s^{-1} at 2 K to ~3 cm^{2}V^{-1}s^{-1} at 250 K, consistent with previous reports on the GAO/STO interface Hall-bar device.[47]

Keeping the pristine properties in mind, we next measured the transport properties of GAO/STO under illumination with different wavelengths (300 nm $\leq \lambda \leq$ 800 nm), as illustrated in Figure 2a. The light covers the whole area of the Hall-bar device. All temperature-dependent R_s curves, plotted in Figure 2b, show well metallic behaviors throughout the whole temperature range unambiguously. Figure 2c shows the underlying mechanism of the optical gating, i.e., the photo-generated electrons can be accumulated in the interfacial 2DEG, resulting in the decrease of resistivity, increase of n_s, and the phenomena discussed later. The wavelength of the applied light ranges from 300 to 800 nm; namely, the photon energy adopted in the present experiment is from ~4.13 to ~1.55 eV. Since the bandgap (E_g) of STO is 3.2 eV, only the light with a wavelength smaller than 387.5 nm could excite the electrons from the valence band (VB) to the conductance band (CB) of STO. Note that, in-gap states at ~−1.2 and −2.1 eV have recently been demonstrated in the GAO/STO hetero-interface to primarily originate from oxygen vacancies.[50] Therefore, electrons confined in in-gap states can also be excited to the CB, because the applied photon energy is larger than 1.55 eV in the present experiment as shown in Figure 2c. This result is consistent with previous reports;[35,37,51,52] i.e., though the adopted photon energy is smaller than E_g, light illumination can excite electrons from the occupied in-gap states in STO to the CB. Moreover, the in-gap states in our GAO/STO interface have already been manifested in transport measurements before optical gating (Figure 1e). In this regard, upon the progressive decrease in the wavelength (equivalently increasing the photon energy), the conductivity of 2DEG was gradually enhanced as expected. For λ decreasing from 800 to
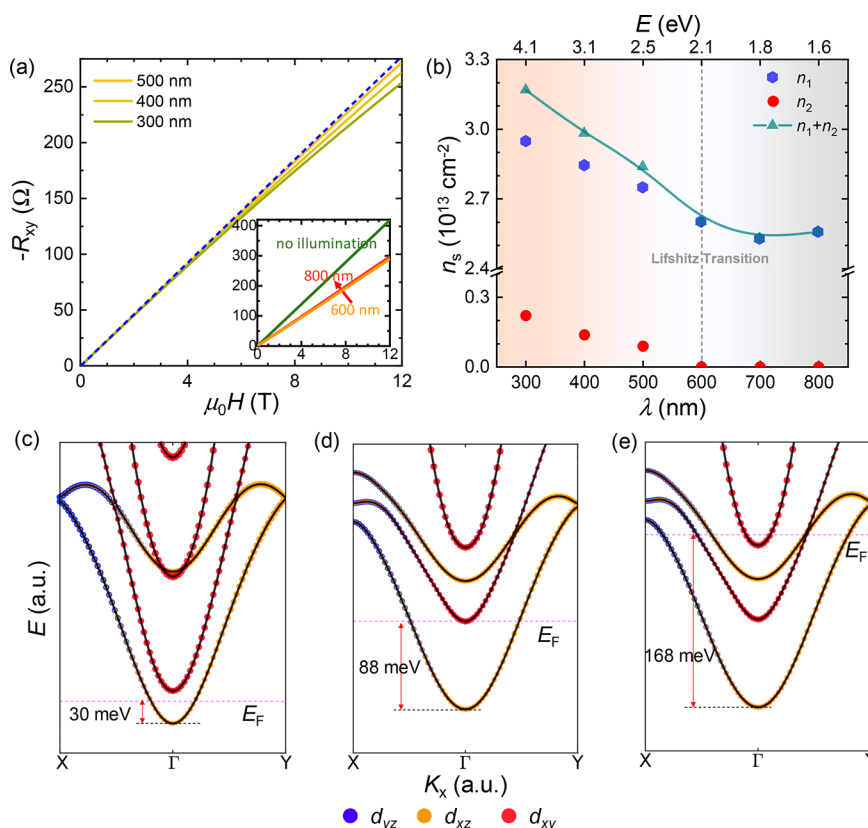
Figure 3. Lifshitz transition in the GAO/STO heterointerface tuned by optical gating. (a) Magnetic field dependence of the nonlinear Hall resistance with λ = 300, 400, and 500 nm, respectively. The dashed line is a linear line for a reference. The inset is the magnetic field dependence of the linear Hall resistance with λ = 600, 700, and 800 nm and no illumination, respectively. (b) The derived carrier densities with respect to the various wavelengths and the corresponding photon energy. (c) The band structure of GAO/STO without illumination. (d) The band structure simulated for λ = 600 nm in which the Lifshitz transition appears. (e) The band structure simulated for λ = 400 nm in which the SOC reaches the maximum. The basic band structure (solid black lines) and the weight of d_{xy} and d_{xz}/d_{yz} (red and orange/blue circles) are calculated from first-principles calculations. The size of the circles represents the weight of the corresponding orbital.

300 nm, the whole temperature-dependent R_s curves showed a downshift (Figure S3a), indicative of an increased number of charge carriers. Particularly, these carrier-concentration enhanced metallic states are more obvious in the low temperature region.

Light intensity provides another knob for optical gating. Figure 2d shows the relative change in resistance ($\Delta R = R - R_b$, where R_b is the balanced resistance after illumination) at 2 K under illumination with λ = 300 nm but different light powers (53−336 μW). It is obvious that the ΔR value is sensitive to the light power. ΔR increases monotonously as the power increases. Despite the largest power adopted in our measurement (336 μW) being relatively smaller than the one used in a previous report,[24] special care should be taken and the measured samples need to be placed at low temperatures for sufficient time to eliminate the heating effect from the applied light irradiation. In addition, as shown in Figure 2d, the resistance of GAO/STO decreases sharply once irradiation begins. In contrast, when turning off the light, the resistance restores slowly to a steady value but is much smaller than the initial one before optical gating, which indicates the typical PPC effect.[32,35] Only when the sample was heated up to room temperature would the resistance return to that of the pristine one.

To quantitatively evaluate the carrier density and the underlying electronic structures, Hall measurements were carried out under illumination. Figure 3a shows field-

dependent R_{xy} in different wavelength regions. As we have shown in Figure 1d, R_{xy} is linear before optical gating. Moreover, starting from the applied longest wavelength of λ = 800 nm to a transition value of λ = 600 nm under optical gating, Hall measurements show a linear dependence of R_{xy} with respect to the magnetic field and R_H is proportional to λ (the inset of Figure 3a). In this wavelength region, a single-band conductivity dominates. Similar to the estimation of intrinsic carrier density, we derive n_s based on $n_s = -1/R_H \cdot e$, which gives $n_s = 2.56 \times 10^{13}$ cm^{-2} at λ = 800 nm and $n_s = 2.60 \times 10^{13}$ cm^{-2} at λ = 600 nm. In contrast, for $\lambda \leq$ 500 nm as shown in Figure 3a, Hall resistances become nonlinear versus the magnetic field, and two distinct slopes are evidenced at low and high magnetic fields, respectively. The appearance of the nonlinear R_{xy} suggests a multicarrier transport scenario, as observed in other oxide 2DEG systems.[15,18,38] The two-band model, therefore, is performed to extract the two carrier densities, n_1 and n_2, from different bands.[26] The carrier density with respect to the wavelength and photon energy is summarized in Figure 3b. In the region of $\lambda \geq$ 600 nm, n_1 electrons dominate exclusively for the conduction and increase slightly with a decrease in λ. For $\lambda \leq$ 500 nm, n_2 carriers begin to emerge. Both n_1 and n_2 carriers increase with a further decrease in λ. A remarkable transition should be noted here at a critical carrier density of ~2.6 × 10^{13} cm^{-2}; the Lifshitz transition induced by a fully optical gating is observed in which new bands with different symmetries are populated, and there
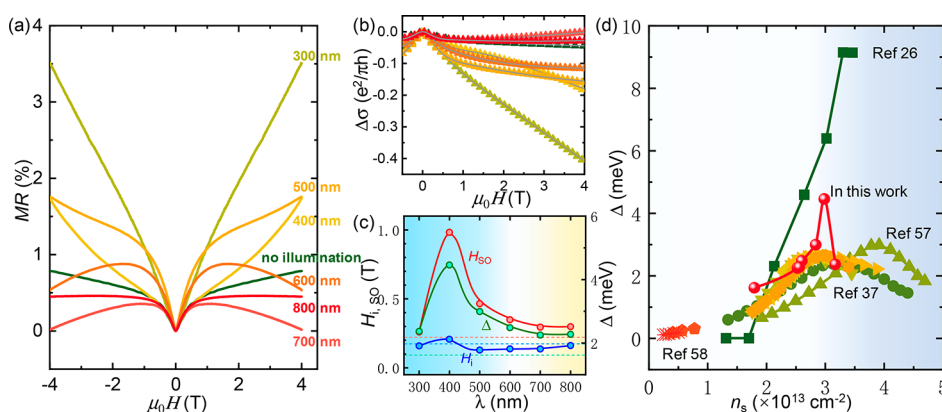
Figure 4. Optical modulation of the Rashba SOC at the GAO/STO interface. (a) Magnetoresistance of the pristine sample and those under illumination with different wavelengths. (b) Normalized magnetoconductivity, $\Delta\sigma$, and the fitting results of the WAL effect. (c) The derived spin−orbit field (H_{SO}), inelastic field (H_i), and Rashba spin splitting energy (Δ) as functions of the wavelengths. Dashed lines indicate the corresponding parameters of the pristine sample before lighting. (d) Carrier density dependence of Rashba spin splitting energy of STO-based 2DEGs, such as GAO/STO,[26] LAO/STO,[37,57,58] and LaVO$_3$/STO.[57]

is concomitant switching from one- to two-carrier transport.[53] Notably, this critical carrier density for the Lifshitz transition is comparable to the one by electrostatic gating (3.0×10^{13} cm^{-2}).[26] Overall, the total carrier density ($n_1 + n_2$) shows an effective tunability (from 1.8 to 3.2×10^{13} cm^{-2}) under the fully optical gating.

As is well established, for STO-based 2DEGs, interfacial electrons originate from t$_{2g}$ bands (d$_{xy}$, d$_{xz}$, and d$_{yz}$) of the Ti 3d orbits.[54] The degeneracy among these three bands is lifted due to tetragonal distortion and quantum confinement.[55] Consequently, an energy splitting between different bands is produced, and carriers therefore can be divided into two categories: d$_{xy}$ and d$_{xz}$/d$_{yz}$ electrons. Unlike the electronic structure of LAO/STO, an unusual orbital ordering, i.e., d$_{xz}$/d$_{yz}$ electrons (rather than d$_{xy}$ ones) occupying the lowest-lying status, was recently proposed in GAO/STO.[42−44] On the basis of this electronic structure, the observed Lifshitz transition can be well understood by the newly populating d$_{xy}$ band (detailed analysis below). Therefore, fully optical gating can drive the modulation of electronic structure and the resultant Lifshitz transition.

To understand the significant tunability of the band structure and Fermi level, we calculated the electronic structure of the GAO/STO heterostructure using first-principles density functional theory (DFT) calculations plus Hubbard U (see Methods for details). The Fermi level was determined by integrating the DFT+U calculated density of states of conduction electrons with respect to the experimentally measured carrier density in Figure 3b. Note that the conduction band minimum is chosen as the zero energy and is shown in Figure 3c−e using a horizontal black dashed line, and the Fermi level is shown by a horizontal magenta line. Before irradiation, the Fermi level is found to be around 30 meV by DFT+U (U = 6 eV) calculations (Figure 3c), and the Fermi level is indeed dominated by the lowest energy states of d$_{xz}$/d$_{yz}$, rather than d$_{xy}$, which reproduces the orbital anomaly of GAO/STO reported in recent studies.[44] In addition, our DFT+U calculations also confirm the latest experimental observation that there is hybridization between the near-Fermi level states of d$_{xz}$ and d$_{yz}$;[44] such hybridization is absent at the LAO/STO interface with C$_{4v}$ symmetry. The strength of hybridization at the GAO/STO interface along Γ−X and Γ−Y k-paths is different, indicating the hybridization is correlated

with the lower symmetry of the complex GAO/STO interface. To simulate the band structure under illumination, we find that Hubbard U should be increased to 8 eV to reproduce the experimentally measured carrier density. It suggests that the electron correlations are very likely to be enhanced under illumination, and it has been believed that the electron correlations play a significant role in electron transport in STO-based systems in the presence of high carrier density.[56] Furthermore, all recent theoretical studies use a very large Hubbard U around 8 eV to study the electronic structure in GAO/STO.[42−44] Therefore, it is practical to use DFT+U (U = 8 eV) calculations to indirectly simulate the illumination effect. In addition, the Fermi level shift in Figure 3d,e is treated in rigid band approximation to address the effect of the wavelength of light. In this way, the modulation of electronic structures and the Fermi level shift can both be simulated under optical gating. Specifically, in the band structure corresponding to a λ of 600 nm, the second lowest-lying sub-band, in which its minimum at Γ is mostly composed of the d$_{xy}$ states, is substantially shifted up compared to that in Figure 3c. This means the energy level differences between the lowest-lying d$_{xz}$/d$_{yz}$ and d$_{xy}$ orbitals are increased under illumination. The Fermi level is shifted up to 88 meV due to the optical enhancement of the carrier density. Particularly, we find the appearance of a new symmetry of the interfacial bands because the d$_{xy}$ state appears around the Fermi level in addition to the d$_{xz}$/d$_{yz}$ states, indicating the Lifshitz transition. Above this Lifshitz transition, interfacial states are composed of the d$_{xz}$/d$_{yz}$ states and d$_{xy}$ states, echoing the occurrence of n_2 carriers in addition to the n_1 carriers as we discussed in Figure 3b. As λ is further reduced to 400 nm, the Fermi level is further shifted up to 168 meV (see Figure 3e).

In addition to the carrier density and the remarkable Lifshitz transition, fully optical gating can also lead to a tunability on the Rashba SOC. To reveal the modulation of Rashba SOC via optical gating, MR measurements of the 2DEG are performed. In Figure 4a, we plot the magnetic field-dependent MR under optical gating with various wavelengths. These MR curves change with a progressive increase in the wavelengths, which is indicative of tunability via optical gating. Most remarkably, it is the same with the pristine MR without illumination: all MR curves show sharp cusps in the low magnetic field region, which is the typical characteristic of the WAL effect due to the

Rashba SOC. For the MR curves with $\lambda \leq 500$ nm as well as the pristine MR before gating, positive MR is observed throughout the whole magnetic field. In contrast, for optical gating with relatively long wavelengths ($\lambda \geq 600$ nm), MR curves show a rapid increase (WAL effect) and then a gradual decrease upon an increase in the magnetic field, i.e., a typical weak localization (WL) effect. Besides the WAL effect, the WL effect can also be observed when the 2DEG is weakly excited ($\lambda \geq 600$ nm). This indicates a switch from destructive to constructive interference of electron waves propagating in time-reversal closed trajectories. In Figure 4b, relative magnetoconductance, $\Delta\sigma = \sigma(H) - \sigma(0)$, is plotted in the unit of $\sigma_0 = e^2/\pi h$.

To fully demonstrate the modulation of Rashba SOC and the underlying electronic structure by optical gating, the WAL/WL effect was analyzed using the modified Maekawa-Fukuyama (MF) theory with a negligible Zeeman effect as previously applied:[3,24]

$$\frac{\Delta\sigma(H)}{\sigma_0} = -\Psi\left(\frac{1}{2} + \frac{H_e}{H}\right) + \frac{3}{2}\Psi\left(\frac{1}{2} + \frac{H_i + H_{so}}{H}\right)$$
$$- \frac{1}{2}\Psi\left(\frac{1}{2} + \frac{H_i}{H}\right) - \left[\ln\left(\frac{H_i + H_{so}}{H_e}\right) + \frac{1}{2}\ln\left(\frac{H_i + H_{so}}{H_i}\right)\right]$$
$$- A_K\frac{\sigma(0)}{\sigma_0}\frac{H^2}{1 + cH^2} \tag{1}$$

where $\Psi(x)$ is the digamma function, H_e, H_i, and H_{so} are the characteristic elastic and inelastic scattering fields and SOC field, respectively. The last term of eq 1 comes from the Kohler term. The fitting results are shown in Figure 4b by the solid lines, attesting a remarkable agreement between the experimental data and localization theory. Thus, it allows a complete exploration on the relations between Rashba SOC and specific electronic structures.

Analyzing the WAL/WL effect based on MF theory allows us to trace the wavelength dependence, essentially the carrier density, of the inelastic scattering field (H_i) and SOC field (H_{so}), as displayed in Figure 4c. H_{so} shows a strong dependence of the gating wavelength, corresponding to the carrier density. Specifically, H_{so} increases from ~0.3 T initially with a decrease in the wavelength (increasing the carrier density). It reaches a peak of ~1 T at $\lambda = 400$ nm and is then immediately followed by a dramatic decrease. These values of characteristic SOC fields are in line with previously reported ones in other oxide 2DEGs.[3,59,60] In contrast, H_i displays a nearly wavelength-independent behavior and varies slightly around the initial value. It is noted that, although the WL effect begins to emerge when $\lambda \geq 600$ nm, H_{so} is larger than H_i all along for the whole optical gating wavelength range, indicating the Rashba SOC is strong enough and the WAL effect plays a dominant role. This could be further proved by the spin relaxation length (L_{so}) and dephasing length (L_i), which are determined by $L_{i,so} = \sqrt{\hbar/(4eH_{i,so})}$. As illustrated in Figure S7a, L_i is longer than L_{so}, consistent with the fact that Rashba SOC dominates in the region.

Furthermore, the Rashba spin splitting energy, Δ, is an indicator of the strength of Rashba SOC. Similar to H_{so}, Δ also shows a considerable tunability via optical gating, which is shown in Figure 4c. Once the 2DEG is illuminated with $\lambda = 800$ nm, Δ increases dramatically from the initial value of ~1.6 to 2.3 meV. When the carrier density is further increased via

optical gating (decreasing λ), Δ increases gradually and reaches a peak of 4.5 meV at $\lambda = 400$ nm and then drops sharply to 2.4 meV. The value of Δ in GAO/STO is comparable to the one of LAO/STO.[3] H_{so} and Δ share the same trend for the optical gating, corresponding to the optical modulation of the electronic structures.

On the basis of the band picture and electronic structures by the optical gating shown in Figure 3c−e, the observed modulation on the Rashba SOC, characterized by H_{so} or Δ, can be unambiguously understood. Before illumination, the Fermi level is around 30 meV above the conduction band bottom. When optical gating is applied with a progressive decrease in the wavelength, the band structure alters and the Fermi level is shifted with the increased carrier density. It has been theoretically demonstrated[61] and experimentally proved[57] that Rashba SOC reaches a maximum at a crossing region between d_{xy} and d_{xz}/d_{yz} bands. Indeed, when the λ decreases from 800 to 400 nm, the Fermi level gets closer to the crossing region; thus, Δ increases gradually. Particularly at $\lambda = 400$ nm, the Fermi level is around 168 meV and is located at the crossing region of the d_{xy} and d_{xz}/d_{yz} bands (see Figure 3e). Therefore, H_{so} and Δ exhibit peaks as in Figure 4c. Subsequently when the Fermi level is increased by decreasing the λ to 300 nm, the Fermi level gets away from the crossing region again. Consequently, Δ shows a drop to 2.4 meV. Furthermore, Δ as a function of the carrier density of STO-based 2DEGs[26,37,57,58] has been summarized in Figure 4d. In the n_s range of 2×10^{12} to 5×10^{13} cm^{-2}, Δ generally increases to a maximum at different n_s and then drops with a further increase in the carrier density. Remarkably, for optical gating, Δ displays a sharp cusp around the crossing region of the d_{xy} and d_{xz}/d_{yz} bands, rather than broad maximums by electrostatic gating. It is also noted that despite some previous papers reported the Rashba SOC was likely to be the strongest around the Lifshitz point;[26,46] our optical gating with a more delicate exploration gives direct evidence that 2DEG systems possess the strongest Rashba SOC at the crossing region between d_{xy} and d_{xz}/d_{yz} bands rather than the Lifshitz transition point. Overall, the Fermi level can be effectively modulated by light irradiation, demonstrating an artificial way of controlling the Rashba SOC.

In conclusion, we have demonstrated an effective modulation of the 2DEG at the GAO/STO heterointerface via fully optical gating. When one only changes the wavelength of the illuminated light, an effectively artificial tuning of the carrier density and underlying electronic structure is realized, during which the 2DEG undergoes a Lifshitz transition and a maximum Rashba SOC. Our present work opens a new pathway for manipulating the emergent properties of the 2DEGs and is promising for all-oxide photoelectric device applications.

■ METHODS

Sample Preparation. GAO thin films were grown on patterned STO substrates by pulsed laser deposition as described elsewhere.[26,47] For a high-quality 2DEG, GAO films were deposited in an oxygen pressure of 1×10^{-5} mbar with an optimal growth temperature of 650 °C. Thickness was controlled by the growth rate, which was calibrated by the reflection high-energy electron diffraction oscillations. On the basis of our previous research, we focused on the GAO/STO heterointerfaces with a thickness of 3 unit cells due to their modest carrier density.[47]

Transport Measurements. Prior to the transport measurements, electrodes were bonded with aluminum wires by means of a wire bonder. Transport properties of the GAO/STO heterointerface devices were measured at temperatures between 2 and 300 K and a perpendicular magnetic field up to 12 T with a CRYOGENIC cryogen-free measurement system. For optical gating during the transport measurements, laser beams (300 nm $\leq \lambda \leq$ 800 nm) were employed into the system. Unless stated otherwise, the laser power was set at 336 μW. Special care should be taken to avoid the heating effect induced by the laser illumination. Notably, after each circle of the optical gating with a certain wavelength, GAO/STO devices were warmed up to 300 K to return to their initial states, eliminating the disturbance from persistent photoconductivity.

Electronic Structure Calculations. The electronic structure was calculated using the first-principles density functional theory (DFT) calculations implemented in the Vienna Ab-initio Simulation Package (VASP).[62,63] We used the Perdew–Burke–Ernzerhof (PBE) exchange-correlation functional plus Dudarev-type[64] Hubbard U method in which the effective U of 6 eV/8 eV for Ti d orbitals was employed. We note that recent theoretical studies also use a large Hubbard U around 8 eV to study the electronic structure in GAO/STO.[44,50] The kinetic energy cutoff was set to be 420 eV. We used the GAO/STO (see Figure S10) superlattice model to simulate the complex spinel/perovskite interface. Since oxygen vacancies were believed to be the origin of 2DEG of GAO/STO, the oxygen defect was created at the interface. The in-plane lattice constants of the structures were constrained onto 3.90 Å, i.e., the experimental lattice constant of STO. The out-of-plane lattice constant and the atomic coordinates along the $x/y/z$ axes were fully optimized until the Hellmann–Feynman forces on each atom were less than 5×10^{-3} eV·Å^{-1}. In the self-consistent field calculations, Brillouin zone integration was sampled using $5 \times 5 \times 1$ k-mesh with a Gaussian smearing of 0.05 eV.

■ ASSOCIATED CONTENT

ⓢ Supporting Information

The Supporting Information is available free of charge at https://pubs.acs.org/doi/10.1021/acs.jpclett.2c00384.

> Detailed description of the methods for sample preparation, transport measurements, and electronic structure calculations, photoinduced changes in resistance, optical modulation, Hall coefficient, high angle annular dark field- and ABF-STEM images, carrier mobility, spin precession distance, dephasing length, diffusion coefficient, spin relaxation time, inelastic scattering time, elastic scattering time, Rashba constant, spin-orbit, inelastic, and elastic fields, magnetic field-dependent magnetoresistance, and optimized structure of spinel/perovskite superlattice (PDF)

■ AUTHOR INFORMATION

Corresponding Authors

Yong Pu − *New Energy Technology Engineering Laboratory of Jiangsu Province and School of Science, Nanjing University of Posts and Telecommunications, Nanjing 210023, China;* Email: puyong@njupt.edu.cn

Yunzhong Chen − *Beijing National Laboratory for Condensed Matter and Institute of Physics, Chinese Academy of Sciences, Beijing 100190, China;* ⓞ orcid.org/0000-0001-8368-5823; Email: yzchen@iphy.ac.cn

Xuefeng Wang − *Jiangsu Provincial Key Laboratory of Advanced Photonic and Electronic Materials, School of Electronic Science and Engineering, Collaborative Innovation Center of Advanced Microstructures, Nanjing University, Nanjing 210093, P. R. China;* ⓞ orcid.org/0000-0002-3472-7895; Email: xfwang@nju.edu.cn

Authors

Wei Niu − *New Energy Technology Engineering Laboratory of Jiangsu Province and School of Science, Nanjing University of Posts and Telecommunications, Nanjing 210023, China; Jiangsu Provincial Key Laboratory of Advanced Photonic and Electronic Materials, School of Electronic Science and Engineering, Collaborative Innovation Center of Advanced Microstructures, Nanjing University, Nanjing 210093, P. R. China;* ⓞ orcid.org/0000-0002-4331-0928

Yue-Wen Fang − *Laboratory for Materials and Structures and Tokyo Tech World Research Hub Initiative (WRHI), Tokyo Institute of Technology, Yokohama, Kanagawa 226-8503, Japan; NYU-ECNU Institute of Physics, New York University Shanghai, Shanghai 200122, China;* ⓞ orcid.org/0000-0003-3674-7352

Ruxin Liu − *Jiangsu Provincial Key Laboratory of Advanced Photonic and Electronic Materials, School of Electronic Science and Engineering, Collaborative Innovation Center of Advanced Microstructures, Nanjing University, Nanjing 210093, P. R. China*

Zhenqi Wu − *New Energy Technology Engineering Laboratory of Jiangsu Province and School of Science, Nanjing University of Posts and Telecommunications, Nanjing 210023, China*

Yongda Chen − *Jiangsu Provincial Key Laboratory of Advanced Photonic and Electronic Materials, School of Electronic Science and Engineering, Collaborative Innovation Center of Advanced Microstructures, Nanjing University, Nanjing 210093, P. R. China*

Yulin Gan − *Beijing National Laboratory for Condensed Matter and Institute of Physics, Chinese Academy of Sciences, Beijing 100190, China*

Xiaoqian Zhang − *Shenzhen Institute for Quantum Science and Engineering, Southern University of Science and Technology, Shenzhen 518055, China*

Chunhui Zhu − *College of Physics, Hebei Normal University, Shijiazhuang 050024, China*

Lixia Wang − *New Energy Technology Engineering Laboratory of Jiangsu Province and School of Science, Nanjing University of Posts and Telecommunications, Nanjing 210023, China*

Yongbing Xu − *New Energy Technology Engineering Laboratory of Jiangsu Province and School of Science, Nanjing University of Posts and Telecommunications, Nanjing 210023, China; Jiangsu Provincial Key Laboratory of Advanced Photonic and Electronic Materials, School of Electronic Science and Engineering, Collaborative Innovation Center of Advanced Microstructures, Nanjing University, Nanjing 210093, P. R. China*

Complete contact information is available at:
https://pubs.acs.org/10.1021/acs.jpclett.2c00384

Author Contributions

○W.N., Y.-W.F., and R.L. contributed equally to this work.

Notes

The authors declare no competing financial interest.

ACKNOWLEDGMENTS

REFERENCES

(1) Ohtomo, A.; Hwang, H. Y. A High-Mobility Electron Gas at the LaAlO$_3$/SrTiO$_3$ Heterointerface. *Nature* **2004**, *427*, 423.

(2) Zhang, M.; Du, K.; Ren, T.; Tian, H.; Zhang, Z.; Hwang, H. Y.; Xie, Y. A Termination-Insensitive and Robust Electron Gas at the Heterointerface of Two Complex Oxides. *Nat. Commun.* **2019**, *10*, 4026.

(3) Caviglia, A. D.; Gabay, M.; Gariglio, S.; Reyren, N.; Cancellieri, C.; Triscone, J. M. Tunable Rashba Spin-Orbit Interaction at Oxide Interfaces. *Phys. Rev. Lett.* **2010**, *104*, 126803.

(4) Ben Shalom, M.; Sachs, M.; Rakhmilevitch, D.; Palevski, A.; Dagan, Y. Tuning Spin-Orbit Coupling and Superconductivity at the SrTiO$_3$/LaAlO$_3$ Interface: A Magnetotransport Study. *Phys. Rev. Lett.* **2010**, *104*, 126802.

(5) Zhang, H.; Yun, Y.; Zhang, X.; Zhang, H.; Ma, Y.; Yan, X.; Wang, F.; Li, G.; Li, R.; Khan, T.; Chen, Y.; Liu, W.; Hu, F.; Liu, B.; Shen, B.; Han, W.; Sun, J. High-Mobility Spin-Polarized Two-Dimensional Electron Gases at Euo/KTaO$_3$ Interfaces. *Phys. Rev. Lett.* **2018**, *121*, 116803.

(6) Reyren, N.; Thiel, S.; Caviglia, A. D.; Kourkoutis, L. F.; Hammerl, G.; Richter, C.; Schneider, C. W.; Kopp, T.; Rüetschi, A.-S.; Jaccard, D.; Gabay, M.; Muller, D. A.; Triscone, J.-M.; Mannhart, J. Superconducting Interfaces between Insulating Oxides. *Science* **2007**, *317*, 1196.

(7) Trier, F.; Prawiroatmodjo, G. E.; Zhong, Z.; Christensen, D. V.; von Soosten, M.; Bhowmik, A.; Lastra, J. M.; Chen, Y.; Jespersen, T. S.; Pryds, N. Quantization of Hall Resistance at the Metallic Interface between an Oxide Insulator and SrTiO$_3$. *Phys. Rev. Lett.* **2016**, *117*, 096804.

(8) Briggeman, M.; Tomczyk, M.; Tian, B.; Lee, H.; Lee, J.-W.; He, Y.; Tylan-Tyler, A.; Huang, M.; Eom, C.-B.; Pekker, D.; Mong, R. S. K.; Irvin, P.; Levy, J. Pascal Conductance Series in Ballistic One-Dimensional LaAlO$_3$/SrTiO$_3$ Channels. *Science* **2020**, *367*, 769−772.

(9) McCollam, A.; Wenderich, S.; Kruize, M. K.; Guduru, V. K.; Molegraaf, H. J. A.; Huijben, M.; Koster, G.; Blank, D. H. A.; Rijnders, G.; Brinkman, A.; Hilgenkamp, H.; Zeitler, U.; Maan, J. C. Quantum Oscillations and Subband Properties of the Two-Dimensional Electron Gas at the LaAlO$_3$/SrTiO$_3$ Interface. *APL Mater.* **2014**, *2*, 022102.

(10) Noël, P.; Trier, F.; Arche, L. M. V.; Bréhin, J.; Vaz, D. C.; Garcia, V.; Fusil, S.; Barthélémy, A.; Vila, L.; Bibes, M.; Attané, J.-P. Non-Volatile Electric Control of Spin−Charge Conversion in a SrTiO$_3$ Rashba System. *Nature* **2020**, *580*, 483.

(11) Ohya, S.; Araki, D.; Anh, L. D.; Kaneta, S.; Seki, M.; Tabata, H.; Tanaka, M. Efficient Intrinsic Spin-to-Charge Current Conversion in an All-Epitaxial Single-Crystal Perovskite-Oxide Heterostructure of La$_{0.67}$Sr$_{0.33}$MnO$_3$/LaAlO$_3$/SrTiO$_3$. *Phys. Rev. Research* **2020**, *2*, 012014R.

(12) Song, Q.; Zhang, H.; Su, T.; Yuan, W.; Chen, Y.; Xing, W.; Shi, J.; Sun, J.; Han, W. Observation of Inverse Edelstein Effect in Rashba-Split 2DEG between SrTiO$_3$ and LaAlO$_3$ at Room Temperature. *Sci. Adv.* **2017**, *3*, e1602312.

(13) Christensen, D. V.; Trier, F.; Niu, W.; Gan, Y.; Zhang, Y.; Jespersen, T. S.; Chen, Y.; Pryds, N. Stimulating Oxide Heterostructures: A Review on Controlling SrTiO$_3$-Based Heterointerfaces with External Stimuli. *Adv. Mater. Interfaces* **2019**, *6*, 1900772.

(14) Zhang, F.; Lv, P.; Zhang, Y.; Huang, S.; Wong, C. M.; Yau, H. M.; Chen, X.; Wen, Z.; Jiang, X.; Zeng, C.; Hong, J.; Dai, J. Y. Modulating the Electrical Transport in the Two-Dimensional Electron Gas at LaAlO$_3$/SrTiO$_3$ Heterostructures by Interfacial Flexoelectricity. *Phys. Rev. Lett.* **2019**, *122*, 257601.

(15) Maniv, E.; Ben Shalom, M.; Ron, A.; Mograbi, M.; Palevski, A.; Goldstein, M.; Dagan, Y. Strong Correlations Elucidate the Electronic Structure and Phase Diagram of LaAlO$_3$/SrTiO$_3$ Interface. *Nat. Commun.* **2015**, *6*, 8239.

(16) Lei, Y.; Li, Y.; Chen, Y. Z.; Xie, Y. W.; Chen, Y. S.; Wang, S. H.; Wang, J.; Shen, B. G.; Pryds, N.; Hwang, H. Y.; Sun, J. R. Visible-Light-Enhanced Gating Effect at the LaAlO$_3$/SrTiO$_3$ Interface. *Nat. Commun.* **2014**, *5*, 5554.

(17) Yan, H.; Zhang, Z.; Wang, S.; Jin, K. Review of Photo-responsive Properties at SrTiO$_3$-Based Heterointerfaces. *Chin. Phys. B* **2018**, *27*, 117804.

(18) Gan, Y.; Christensen, D. V.; Zhang, Y.; Zhang, H.; Krishnan, D.; Zhong, Z.; Niu, W.; Carrad, D. J.; Norrman, K.; von Soosten, M.; Jespersen, T. S.; Shen, B.; Gauquelin, N.; Verbeeck, J.; Sun, J.; Pryds, N.; Chen, Y. Diluted Oxide Interfaces with Tunable Ground States. *Adv. Mater.* **2019**, *31*, 1805970.

(19) Fix, T.; Schoofs, F.; MacManus-Driscoll, J. L.; Blamire, M. G. Influence of Doping at the Nanoscale at LaAlO$_3$/SrTiO$_3$ Interfaces. *Appl. Phys. Lett.* **2010**, *97*, 072110.

(20) Christensen, D. V.; Trier, F.; von Soosten, M.; Prawiroatmodjo, G. E. D. K.; Jespersen, T. S.; Chen, Y. Z.; Pryds, N. Electric Field Control of the γ-Al$_2$O$_3$/SrTiO$_3$ Interface Conductivity at Room Temperature. *Appl. Phys. Lett.* **2016**, *109*, 021602.

(21) Bell, C.; Harashima, S.; Kozuka, Y.; Kim, M.; Kim, B. G.; Hikita, Y.; Hwang, H. Y. Dominant Mobility Modulation by the Electric Field Effect at the LaAlO$_3$/SrTiO$_3$ Interface. *Phys. Rev. Lett.* **2009**, *103*, 226802.

(22) Thiel, S.; Hammerl, G.; Schmehl, A.; Schneider, C. W.; Mannhart, J. Tunable Quasi−Two-Dimensional Electron Gases in Oxide Heterostructures. *Science* **2006**, *313*, 1942.

(23) Yin, C.; Smink, A. E. M.; Leermakers, I.; Tang, L. M. K.; Lebedev, N.; Zeitler, U.; van der Wiel, W. G.; Hilgenkamp, H.; Aarts, J. Electron Trapping Mechanism in LaAlO$_3$/SrTiO$_3$ Heterostructures. *Phys. Rev. Lett.* **2020**, *124*, 017702.

(24) Zhang, H.; Yan, X.; Zhang, X.; Wang, S.; Xiong, C.; Zhang, H.; Qi, S.; Zhang, J.; Han, F.; Wu, N.; Liu, B. G.; Chen, Y.; Shen, B.; Sun, J. Unusual Electric and Optical Tuning to KTaO$_3$-Based Two-Dimensional Electron Gases with 5*d* Orbitals. *ACS Nano* **2019**, *13*, 609−615.

(25) Caviglia, A. D.; Gariglio, S.; Reyren, N.; Jaccard, D.; Schneider, T.; Gabay, M.; Thiel, S.; Hammerl, G.; Mannhart, J.; Triscone, J. M. Electric Field Control of the LaAlO$_3$/SrTiO$_3$ Interface Ground State. *Nature* **2008**, *456*, 624−627.

(26) Niu, W.; Zhang, Y.; Gan, Y.; Christensen, D. V.; Soosten, M. V.; Garcia-Suarez, E. J.; Riisager, A.; Wang, X.; Xu, Y.; Zhang, R.; Pryds, N.; Chen, Y. Giant Tunability of the Two-Dimensional Electron Gas at the Interface of γ-Al$_2$O$_3$/SrTiO$_3$. *Nano Lett.* **2017**, *17*, 6878−6885.

(27) Pena, V.; Gredig, T.; Santamaria, J.; Schuller, I. K. Interfacially Controlled Transient Photoinduced Superconductivity. *Phys. Rev. Lett.* **2006**, *97*, 177005.

(28) Lin, J. C.; Tra, V. T.; Tsai, D. S.; Lin, T. T.; Huang, P. C.; Hsu, W. L.; Wu, H. J.; Huang, R.; Van Chien, N.; Yoshida, R.; Lin, J. Y.; Ikuhara, Y.; Chiu, Y. P.; Gwo, S.; Tsai, D. P.; He, J. H.; Chu, Y. H. Control of the Metal-Insulator Transition at Complex Oxide

Heterointerfaces through Visible Light. *Adv. Mater.* **2016**, *28*, 764−770.

(29) Matsubara, M.; Okimoto, Y.; Ogasawara, T.; Tomioka, Y.; Okamoto, H.; Tokura, Y. Ultrafast Photoinduced Insulator-Ferromagnet Transition in the Perovskite Manganite $Gd_{0.55}Sr_{0.45}MnO_3$. *Phys. Rev. Lett.* **2007**, *99*, 207401.

(30) Leermakers, I.; Rubi, K.; Yang, M.; Kerdi, B.; Goiran, M.; Escoffier, W.; Rana, A. S.; Smink, A. E. M.; Brinkman, A.; Hilgenkamp, H.; Maan, J. C.; Zeitler, U. Quantum Oscillations in an Optically-Illuminated Two-Dimensional Electron System at the $LaAlO_3/SrTiO_3$ Interface. *J. Phys.: Condens. Matter* **2021**, *33*, 465002.

(31) Press, D.; Ladd, T. D.; Zhang, B.; Yamamoto, Y. Complete Quantum Control of a Single Quantum Dot Spin Using Ultrafast Optical Pulses. *Nature* **2008**, *456*, 218−221.

(32) Tebano, A.; Fabbri, E.; Pergolesi, D.; Balestrino, G.; Traversa, E. Room-Temperature Giant Persistent Photoconductivity in $SrTiO_3/LaAlO_3$ Heterostructures. *ACS Nano* **2012**, *6*, 1278−1283.

(33) Liu, H.-J.; Wang, J.-C.; Cho, D.-Y.; Ho, K.-T.; Lin, J.-C.; Huang, B.-C.; Fang, Y.-W.; Zhu, Y.-M.; Zhan, Q.; Xie, L.; Pan, X.-Q.; Chiu, Y.-P.; Duan, C.-G.; He, J.-H.; Chu, Y.-H. Giant Photoresponse in Quantized $SrRuO_3$ Monolayer at Oxide Interfaces. *ACS Photonics* **2018**, *5*, 1041−1049.

(34) V, A.; Kumar, P.; Pal, P.; Dogra, A. Photo-Resistive Properties of $LaAl_{0.6}Cr_{0.4}O_3/SrTiO_3$ Heterostructures: A Comparative Study with $LaAlO_3/SrTiO_3$. *Opt. Lett.* **2016**, *41*, 1134−1137.

(35) Di Gennaro, E.; di Uccio, U. S.; Aruta, C.; Cantoni, C.; Gadaleta, A.; Lupini, A. R.; Maccariello, D.; Marré, D.; Pallecchi, I.; Paparo, D.; Perna, P.; Riaz, M.; Granozio, F. M. Persistent Photoconductivity in 2D Electron Gases at Different Oxide Interfaces. *Advanced Optical Materials* **2013**, *1*, 834−843.

(36) Yan, H.; Zhang, Z.; Wang, S.; Wei, X.; Chen, C.; Jin, K. Magnetism Control by Doping in $LaAlO_3/SrTiO_3$ Heterointerfaces. *ACS Appl. Mater. Interfaces* **2018**, *10*, 14209−14213.

(37) Cheng, L.; Wei, L.; Liang, H.; Yan, Y.; Cheng, G.; Lv, M.; Lin, T.; Kang, T.; Yu, G.; Chu, J.; Zhang, Z.; Zeng, C. Optical Manipulation of Rashba Spin-Orbit Coupling at $SrTiO_3$-Based Oxide Interfaces. *Nano Lett.* **2017**, *17*, 6534.

(38) Smink, A. E.; de Boer, J. C.; Stehno, M. P.; Brinkman, A.; van der Wiel, W. G.; Hilgenkamp, H. Gate-Tunable Band Structure of the $LaAlO_3$-$SrTiO_3$ Interface. *Phys. Rev. Lett.* **2017**, *118*, 106401.

(39) Chen, Y. Z.; Bovet, N.; Trier, F.; Christensen, D. V.; Qu, F. M.; Andersen, N. H.; Kasama, T.; Zhang, W.; Giraud, R.; Dufouleur, J.; Jespersen, T. S.; Sun, J. R.; Smith, A.; Nygard, J.; Lu, L.; Buchner, B.; Shen, B. G.; Linderoth, S.; Pryds, N. A High-Mobility Two-Dimensional Electron Gas at the Spinel/Perovskite Interface of γ-$Al_2O_3/SrTiO_3$. *Nat. Commun.* **2013**, *4*, 1371.

(40) Varignon, J.; Vila, L.; Barthélémy, A.; Bibes, M. A New Spin for Oxide Interfaces. *Nat. Phys.* **2018**, *14*, 322−325.

(41) Christensen, D. V.; Frenkel, Y.; Chen, Y. Z.; Xie, Y. W.; Chen, Z. Y.; Hikita, Y.; Smith, A.; Klein, L.; Hwang, H. Y.; Pryds, N.; Kalisky, B. Strain-Tunable Magnetism at Oxide Domain Walls. *Nat. Phys.* **2019**, *15*, 269−274.

(42) Cao, Y.; Liu, X.; Shafer, P.; Middey, S.; Meyers, D.; Kareev, M.; Zhong, Z.; Kim, J.-W.; Ryan, P. J.; Arenholz, E.; Chakhalian, J. Anomalous Orbital Structure in a Spinel−Perovskite Interface. *npj Quantum Mater.* **2016**, *1*, 16009.

(43) Mardegan, J. R. L.; Christensen, D. V.; Chen, Y. Z.; Parchenko, S.; Avula, S. R. V.; Ortiz-Hernandez, N.; Decker, M.; Piamonteze, C.; Pryds, N.; Staub, U. Magnetic and Electronic Properties at the γ-$Al_2O_3/SrTiO_3$ Interface. *Phys. Rev. B* **2019**, *99*, 134423.

(44) Chikina, A.; Christensen, D. V.; Borisov, V.; Husanu, M. A.; Chen, Y.; Wang, X.; Schmitt, T.; Radovic, M.; Nagaosa, N.; Mishchenko, A. S.; Valenti, R.; Pryds, N.; Strocov, V. N. Band-Order Anomaly at the γ-$Al_2O_3/SrTiO_3$ Interface Drives the Electron-Mobility Boost. *ACS Nano* **2021**, *15*, 4347−4356.

(45) Huijben, M.; Brinkman, A.; Koster, G.; Rijnders, G.; Hilgenkamp, H.; Blank, D. H. A. Structure-Property Relation of $SrTiO_3/LaAlO_3$ Interfaces. *Adv. Mater.* **2009**, *21*, 1665−1677.

(46) Gan, Y.; Zhang, Y.; Christensen, D. V.; Pryds, N.; Chen, Y. Gate-Tunable Rashba Spin-Orbit Coupling and Spin Polarization at Diluted Oxide Interfaces. *Phys. Rev. B* **2019**, *100*, 125134.

(47) Niu, W.; Gan, Y.; Zhang, Y.; Christensen, D. V.; von Soosten, M.; Wang, X.; Xu, Y.; Zhang, R.; Pryds, N.; Chen, Y. Suppressed Carrier Density for the Patterned High Mobility Two-Dimensional Electron Gas at γ-$Al_2O_3/SrTiO_3$ Heterointerfaces. *Appl. Phys. Lett.* **2017**, *111*, 021602.

(48) Shibuya, K.; Ohnishi, T.; Uozumi, T.; Sato, T.; Nishio, K.; Lippmaa, M. Observation of $SrTiO_3$ in-Gap States by Depletion Mode Field Effect. *Appl. Phys. Lett.* **2008**, *92*, 032109.

(49) Zeng, S. W.; Yin, X. M.; Herng, T. S.; Han, K.; Huang, Z.; Zhang, L. C.; Li, C. J.; Zhou, W. X.; Wan, D. Y.; Yang, P.; Ding, J.; Wee, A. T. S.; Coey, J. M. D.; Venkatesan, T.; Rusydi, A.; Ariando, A. Oxygen Elelctromigration and Energy Band Reconstruction Induced by Electrolyte Field Effect at Oxide Interfaces. *Phys. Rev. Lett.* **2018**, *121*, 146802.

(50) Schütz, P.; Christensen, D. V.; Borisov, V.; Pfaff, F.; Scheiderer, P.; Dudy, L.; Zapf, M.; Gabel, J.; Chen, Y. Z.; Pryds, N.; Rogalev, V. A.; Strocov, V. N.; Schlueter, C.; Lee, T. L.; Jeschke, H. O.; Valentí, R.; Sing, M.; Claessen, R. Microscopic Origin of the Mobility Enhancement at a Spinel/Perovskite Oxide Heterointerface Revealed by Photoemission Spectroscopy. *Phys. Rev. B* **2017**, *96*, 161409R.

(51) Wang, X.; Chen, J. Q.; Barman, A. R.; Dhar, S.; Xu, Q.-H.; Venkatesan, T.; Ariando. Static and Ultrafast Dynamics of Defects of $SrTiO_3$ in $LaAlO_3/SrTiO_3$ Heterostructures. *Appl. Phys. Lett.* **2011**, *98*, 081916.

(52) Lu, H. L.; Liao, Z. M.; Zhang, L.; Yuan, W. T.; Wang, Y.; Ma, X. M.; Yu, D. P. Reversible Insulator-Metal Transition of $LaAlO_3/SrTiO_3$ Interface for Nonvolatile Memory. *Sci. Rep* **2013**, *3*, 2870.

(53) Joshua, A.; Pecker, S.; Ruhman, J.; Altman, E.; Ilani, S. A Universal Critical Density Underlying the Physics of Electrons at the $LaAlO_3/SrTiO_3$ Interface. *Nat. Commun.* **2012**, *3*, 1129.

(54) Gabay, M.; Triscone, J.-M. Hund Rules with a Twist. *Nat. Phys.* **2013**, *9*, 610−611.

(55) Santander-Syro, A. F.; Copie, O.; Kondo, T.; Fortuna, F.; Pailhes, S.; Weht, R.; Qiu, X. G.; Bertran, F.; Nicolaou, A.; Taleb-Ibrahimi, A.; Le Fevre, P.; Herranz, G.; Bibes, M.; Reyren, N.; Apertet, Y.; Lecoeur, P.; Barthelemy, A.; Rozenberg, M. J. Two-Dimensional Electron Gas with Universal Subbands at the Surface of $SrTiO_3$. *Nature* **2011**, *469*, 189−193.

(56) Lee, M.; Williams, J. R.; Zhang, S.; Frisbie, C. D.; Goldhaber-Gordon, D. Electrolyte Gate-Controlled Kondo Effect in $SrTiO_3$. *Phys. Rev. Lett.* **2011**, *107*, 256601.

(57) Liang, H.; Cheng, L.; Wei, L.; Luo, Z.; Yu, G.; Zeng, C.; Zhang, Z. Nonmonotonically Tunable Rashba Spin-Orbit Coupling by Multiple-Band Filling Control in $SrTiO_3$-Based Interfaciald-Electron Gases. *Phys. Rev. B* **2015**, *92*, 075309.

(58) Nakamura, H.; Koga, T.; Kimura, T. Experimental Evidence of Cubic Rashba Effect in an Inversion-Symmetric Oxide. *Phys. Rev. Lett.* **2012**, *108*, 206601.

(59) Herranz, G.; Singh, G.; Bergeal, N.; Jouan, A.; Lesueur, J.; Gazquez, J.; Varela, M.; Scigaj, M.; Dix, N.; Sanchez, F.; Fontcuberta, J. Engineering Two-Dimensional Superconductivity and Rashba Spin-Orbit Coupling in $LaAlO_3/SrTiO_3$ Quantum Wells by Selective Orbital Occupancy. *Nat. Commun.* **2015**, *6*, 6028.

(60) Das, S.; Hossain, Z.; Budhani, R. C. Signature of Enhanced Spin-Orbit Interaction in the Magnetoresistance of $LaAlO_3/SrTiO_3$ Interfaces on Δ Doping. *Phys. Rev. B* **2016**, *94*, 115165.

(61) Zhong, Z.; Tóth, A.; Held, K. Theory of Spin-Orbit Coupling at $LaAlO_3/SrTiO_3$ Interfaces and $SrTiO_3$ Surfaces. *Phys. Rev. B* **2013**, *87*, 161102R.

(62) Kresse, G.; Furthmüller, J. Efficiency of Ab-Initio Total Energy Calculations for Metals and Semiconductors Using a Plane-Wave Basis Set. *Comput. Mater. Sci.* **1996**, *6*, 15−50.

(63) Kresse, G.; Furthmuller, J. Efficient Iterative Schemes for Ab Initio Total-Energy Calculations Using a Plane-Wave Basis Set. *Phys. Rev. B* **1996**, *54*, 11169.

(64) Dudarev, S. L.; Botton, G. A.; Savrasov, S. Y.; Humphreys, C. J.; Sutton, A. P. Electron-Energy-Loss Spectra and the Structural Stability of Nickel Oxide: An Lsda+U Study. *Phys. Rev. B* **1998**, *57*, 1505−1509.

📖 Recommended by ACS

Giant Bandgap Engineering in Two-Dimensional Ferroelectric α-In₂Se₃

Jiaxiang Zhang, Lan Chen, *et al.*

APRIL 07, 2022
THE JOURNAL OF PHYSICAL CHEMISTRY LETTERS

READ 🗗

Nearly Ideal Two-Dimensional Electron Gas Hosted by Multiple Quantized Kronig–Penney States Observed in Few-Layer InSe

Yu Wang, Lan Chen, *et al.*

AUGUST 09, 2022
ACS NANO

READ 🗗

Contact Properties of Two-Dimensional Ferroelectric α-In₂Se₃

Bo Liu, Qing Chen, *et al.*

OCTOBER 11, 2021
ACS APPLIED ELECTRONIC MATERIALS

READ 🗗

Modulation of the Metal–Nonmetal Crossover in SrIrO₃/CaMnO₃ Superlattices

Minghui Gu, Jiandong Guo, *et al.*

JULY 15, 2022
ACS APPLIED ELECTRONIC MATERIALS

READ 🗗

Get More Suggestions >